

Northumbria Research Link

Citation: Zhu, Qingsong, Zhao, Yao, Miao, Baoji, Abo-Dief, Hala M., Qu, Muchao, Pashameah, Rami Adel, Xu, Bin, Huang, Mina, Algadi, Hassan, Liu, Xianhu and Guo, Zhanhu (2022) Hydrothermally synthesized ZnO-RGO-PPy for water-borne epoxy nanocomposite coating with anticorrosive reinforcement. Progress in Organic Coatings, 172. p. 107153. ISSN 0033-0655

Published by: Elsevier

URL: <https://doi.org/10.1016/j.porgcoat.2022.107153>
<<https://doi.org/10.1016/j.porgcoat.2022.107153>>

This version was downloaded from Northumbria Research Link:
<https://nrl.northumbria.ac.uk/id/eprint/49947/>

Northumbria University has developed Northumbria Research Link (NRL) to enable users to access the University's research output. Copyright © and moral rights for items on NRL are retained by the individual author(s) and/or other copyright owners. Single copies of full items can be reproduced, displayed or performed, and given to third parties in any format or medium for personal research or study, educational, or not-for-profit purposes without prior permission or charge, provided the authors, title and full bibliographic details are given, as well as a hyperlink and/or URL to the original metadata page. The content must not be changed in any way. Full items must not be sold commercially in any format or medium without formal permission of the copyright holder. The full policy is available online: <http://nrl.northumbria.ac.uk/policies.html>

This document may differ from the final, published version of the research and has been made available online in accordance with publisher policies. To read and/or cite from the published version of the research, please visit the publisher's website (a subscription may be required.)

Hydrothermally synthesized ZnO-RGO-PPy for water-borne epoxy nanocomposite coating with anticorrosive reinforcement

Qingsong Zhu¹, Yao Zhao¹, Baoji Miao^{1*}, Hala M. Abo-Dief², Muchao Qu^{3,4}, Rami Adel Pashameah⁵, Ben Bin Xu⁷, Mina Huang^{8,9}, Hassan Algadi¹⁰, Xianhu Liu^{6*}, Zhanhu Guo^{8*}

School of Material Science and Engineering, Henan International Joint Laboratory of Nano-photoelectric Magnetic Materials, Henan University of Technology, Zhengzhou 450001, China

²Department of Chemistry, College of Science, Taif University, P.O. Box 11099 Taif 21944, Saudi Arabia

³ School of Automobile and Transportation Engineering, Guangdong Polytechnic Normal University, Guangzhou 510450, China

⁴ SCNU Qingyuan Institute of Science and Technology Innovation Co., Ltd., Qingyuan 511517, China

⁵Department of Chemistry, Faculty of Applied Science, Umm Al-Qura University, Makkah 24230, Saudi Arabia

⁶ National Engineering Research Center for Advanced Polymer Processing Technology, Zhengzhou University, Zhengzhou 450002, China

⁷ Department of Mechanical and Construction Engineering, Faculty of Engineering and Environment, Northumbria University, Newcastle upon Tyne, NE1 8ST, UK

⁸ Integrated Composites Laboratory (ICL), Department of Chemical & Biomolecular Engineering, University of Tennessee, Knoxville, TN 37996, USA

⁹ College of Materials Science and Engineering, Taiyuan University of Science and Technology, Taiyuan, 030024, China

¹⁰Department of Electrical Engineering, Faculty of Engineering, Najran University, P.O. Box 1988, Najran 11001, Saudi Arabia

*: Corresponding authors

baoji_miao@haut.edu.cn (B. Miao), xianhu.liu@zzu.edu.cn (X. Liu) or nanomaterials2000@gmail.com (Z. Guo)

Abstract: Waterborne epoxy (WEP) nanocomposite coating with hydrothermal synthesized zinc oxide (ZnO)-reduced graphene oxide (RGO)- polypyrrole (PPy) was prepared and an enhanced corrosion resistance was reported. Experiment results showed that WEP nanocomposite coating with Z8R2P (the mass ratio of ZnO-RGO-PPy of 8:2:1) exhibited the highest value of the impedance at the lowest frequency (such as $|Z|_{0.01\text{Hz}}$), the lowest corrosion current density and the largest value of charge transfer resistance (R_{ct}). Even after 94 days of immersion, the $|Z|_{0.01\text{Hz}}$ value of Z8R2P/WEP nanocomposite coating was $4.45 \times 10^3 \Omega \cdot \text{cm}^2$, pointing out that Z8R2P/WEP coating possessed the long superior anticorrosion performance. Moreover, salt spray experiments with a period of 50 days showed that Z8R2P/WEP coating had the best integrity of coating compared with other coatings, revealing that Z8R2P/WEP coating had the best corrosion protection performance. The characterization and analysis of phase composition and corrosion morphology revealed that the synergistic protection mechanism of Z8R2P/WEP coating was attributed to barrier effects of RGO, chemical passivation of ZnO and accept the released electrons of PPy.

Keywords: Reduced Graphene Oxide; Polypyrrole; Corrosion; Epoxy; Nanocomposites.

1. Introduction

Metals and their alloys have attracted much interests due to their wide applications [1-12] and the easy corrosion has caused serious problems [13-17]. Many methods have been reported to prevent the corrosion [18-20]. Epoxy resin has been widely used in corrosion protection of metal surface due to excellent strong mechanical properties [21-24], corrosion resistance, chemical resistance [25], and

durable adhesion with metal matrix [26-34]. Owing to environmental considerations, waterborne epoxy resin (WEP) has been replacing solvent-borne epoxy resin in anticorrosive coatings fields [35-37]. Surfactants and hydrophilic groups are usually used to prepare WEP emulsion. Residual surfactants and hydrophilic groups in the curing process will lead to the micro-pores and defects in the coating, decrease the water-resistance of the coating, as well as the corrosion resistance [38, 39]. Hence, exploring new strategies and technologies to improve the corrosion protection of WEP coating is urgent.

Alkali metal oxide is usually used in the WEP coating for corrosion resistance on the metal surface. For example, ZnO has good ultraviolet shield effect [40-42], forms dense zinc-iron compounds on the surface between the coating and metal matrix, reduces the penetration rate of corrosive media. For example, Rahman *et al.* added ZnO nanoparticles into epoxy-polyamide matrix. Results revealed that the addition of high loading of nanoparticles decreased the glass transition temperature of the composites and increased the coating resistance against hydrolytic degradation [39]. Moreover, Ramezanzadeh *et al.* reported the effects of nano and micron sized ZnO particles on the hydrolytic degradation and corrosion resistance of an epoxy coating. Results showed that the nano-composites exhibited a greater hydrolytic resistance compared to micro-composite [43].

Graphene and its derivatives have excellent barrier reinforcements for epoxy coatings due to its high specific surface area and excellent impermeability [44-48]. However, graphene and its derivatives exhibit a close-packed layered structure owing to their intrinsic van der Waals' interaction and the synthesis procedure consisting of a vacuum filtration, then leading to poor dispersion in epoxy coating [49-54]. To preclude the aggregation of GO nanosheets and to achieve a homogeneous dispersion and enhanced compatibility with epoxy, decorating sheets with inorganic nanoparticles is a facile and efficient approach [50, 55-58]. Moreover, the loading of nanoparticles on the GO surfaces increased

the layer spacing by separating nanosheets efficiently. For example, Pourhashem *et al.* used tetraethyl orthosilicate to decorate the surface of GO nanosheets by SiO₂ nanospheres via a facile method. Then, embedding the well-distributed SiO₂-GO nanohybrids into epoxy coating remarkably enhanced the corrosion resistance compared to GO nanosheets [59]. Yu *et al.* synthesized TiO₂-GO sheet hybrids [60] and Al₂O₃-GO [61] with the help of 3-aminopropyltriethoxysilane, respectively. Embedding the nanosheets into epoxy resin improved the corrosion resistance. In addition, polypyrrole (PPy) has recently been used in the field of anticorrosion coatings due to excellent conductivity and flexibility [62]. Ding *et al.* [63] prepared PPy nanowires/graphene composites through an in-situ polymerization, and improved the corrosion resistance of WEP coatings. Results showed that a high barrier performance of graphene and passivation effect of PPy were conducive to corrosion protection. Qiu *et al.* [50] reported the synergistic effect of PPy-intercalated graphene for enhanced corrosion protection of WEP coatings. Zhu *et al.* [36] prepared the GO-PPy composites through an in-situ polymerization to significantly improve the corrosion resistance of WEP coatings in 3.5% NaCl solution. To the best of our knowledge, using ternary composites ZnO-RGO-PPy to improve the corrosion resistance of WEP coating has not yet been reported.

Herein, the synergistic effect of ZnO-RGO-PPy as a new nanofiller in WEP coating was investigated. ZnO-RGO composites were hydrothermally prepared by metal oxide and GO as precursors. Then Py monomer was added into the synthesized ZnO-RGO as precursors to synthesize ZnO-RGO-PPy composites. The corrosion resistance of ZnO-RGO-PPy/WEP coating were measured by electrochemical impedance spectroscopy (EIS) and salt spray test, and the protective mechanism was revealed by the phase composition and morphology.

2. Experimental

2.1. Materials

Zn(NO₃)₂·6H₂O, KOH, NaCl and ethanol were purchased from Sinopharm Chemical Reagent Co., Ltd. All aqueous solutions were used with deionized water. Waterborne two-component epoxy/amine coating system and corresponding water-borne curing agent were supplied by the epoxy resin department of Baling Petrochemical Co., Ltd. GO were synthesized according to our previous report [5]. The dimension of the mild steel specimens was 120 × 50 × 0.28 mm³, and these chemical compositions (wt%) were: ≤ 0.22 C, ≤ 0.045 P, ≤ 0.70 Mn, ≤ 0.34 Si, ≤ 0.05 S and balance Fe. Prior to coating the steel specimen, mild steel specimens were grinded with 100, 400, 800 grit SiC sandpapers to remove oxide layer, respectively. Then, these specimens were cleaned using ethanol solution.

2.2. Synthesis of ZnO-RGO-PPy

ZnO-RGO-PPy were synthesized by two-step modification. ZnO-RGO was prepared by the hydrothermal synthesis according to our previous report [64]. Then, 0.1077 g ZnO-RGO was added to a breaker containing 100 mL deionized water. The dissolved solution was placed in the cell pulverizer for ultrasonic treatment to obtain a uniformly dispersed suspension system. Subsequently, 0.5 g of sodium dodecylbenzene sulfonate (C₁₈H₂₉NaSO₃) was added to the suspension with continuous stirring in an ice bath. At the same time, 14.4 mmol Py monomer was added into a breaker of 20 mL ethanol solution. After Py was completely dispersed, the solution was translated into the above suspension system, and sonicated for 30 min to absorb Py monomer on the surface of ZnO_RGO. Then, 30 mL of 0.48 M (NH₄)₂S₂O₈ was added to the above suspension and stirred continuously for 24 h in an ice bath. The flocs after hydrothermal reaction were filtered and washed several times with the

mixture solution of deionized water and ethanol (1:1). Finally, the ultimate flocs were placed in a vacuum drying oven and the temperature was maintained at 60 °C for 24 h, the obtained black powder was ZnO-RGO-PPy. Since the mass ratio among ZnO, PPy and GO was 2:2:1, the obtained ZnO-RGO-PPy was recorded as Z2R2P. For comparison, the composites with the mass ratio of ZnO-RGO-PPy of 8:2:1 and 2:6:3 were prepared by the same method and recorded as Z8R2P and Z2R6P3.

2.3. Preparation of ZnO-RGO-PPy/WEP coatings

Fig. 1 represents the schematic diagram of the preparation process of ZnO-RGO-PPy/WEP composite coatings. Typically, 0.504 g of Z8R2P was added to 10 mL deionized water and ultrasonic treatment for 30 min to obtain a uniformly dispersed composite system. Then, 5.2 g of aqueous curing agent was added to the above suspension and stirred magnetically for 30 min. After that, 20 g WEP emulsion was added to the above mixed solution and continued stirring. Then the mixture solution was placed in a vacuum drying oven for 30 min for degassing treatment to eliminate bubbles in the mixture. To maintain the same thickness of the coatings, the wire rod of 80 μm was used to coat the pretreated mild steels and placed the coated steels at room temperature for 24 h. After that, all samples were cured in an electric blow-drying oven for 60, 90 and 120 °C for 2 h, respectively. Finally, the obtained coating was named as Z8R2P/WEP. For comparison, WEP, Z2R2P/WEP, and Z2R6P3/WEP coatings were prepared by the similar methods.

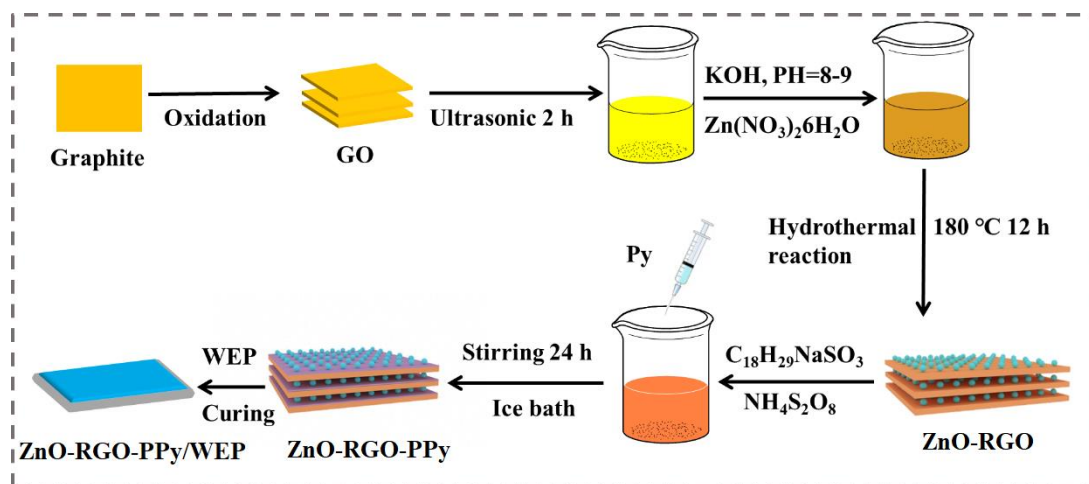


Fig. 1. Schematic diagram of the preparation process of ZnO-RGO-PPy/WEP composite coatings.

2.4. Characterization

The morphologies of the GO, Z2R2P, Z8R2P, Z2R6P3 and these corresponding composite coatings were characterized by field emission scanning electron microscope (FESEM, an Inspect F50 scanning electron microscope). The structure characteristics of GO, Z2R2P, Z8R2P, Z2R6P3 and these corresponding composite coatings were characterized by X-ray diffraction patterns (XRD, Bruker D8 Advance) with Cu K α radiation at 40 mA and 40 kV by a scanning rate of 1° min⁻¹ 14. The Fourier transform infrared (FT-IR) spectra of GO, Z2R2P, Z8R2P and Z2R6P3 were recorded using the Prestige-21 with the range from 400 to 4000 cm⁻¹. Raman spectra of GO, Z2R2P, Z8R2P and Z2R6P3 were obtained from a Nano-finder 30 confocal Raman Microscope (Lab RAM HR Evolution, French) with the range from 50 cm⁻¹ to 3000 cm⁻¹ via a He-Ne laser beam with a wavelength of 532 nm.

The corrosion resistance performances of the composite coatings were tested using an electrochemical impedance spectroscopy (EIS) by an electrochemical workstation (RST5200F, Zhengzhou Shiruisi Instrument Technology Co., Ltd.) with a conventional three-electrode configuration including the work electrode, platinum counter electrode and reference electrode

(Ag/AgCl), and the corrosive electrolyte was the 3.5 wt% NaCl solution. A geometrical area of 12 cm² was used to the electrolytic solution for the work electrode. A scan rate of 1 mV s⁻¹ was carried on the electrochemical workstation to obtain the polarization plots. All EIS measures were run in the frequencies range from 105 to 10⁻² Hz with an amplitude of 5 mV. EIS spectra were fitted using a ZSimpWin software to obtain the equivalent circuit and the key electrochemical parameters. Salt spray test measurements of the composite coatings were conducted in a salt spray chamber according to GB 1771-2007 standards, and the concentration of NaCl solutions was 5 wt%.

3. Results and discussion

3.1. Structure and morphologies of Z2R2P, Z8R2P and Z2R6P3

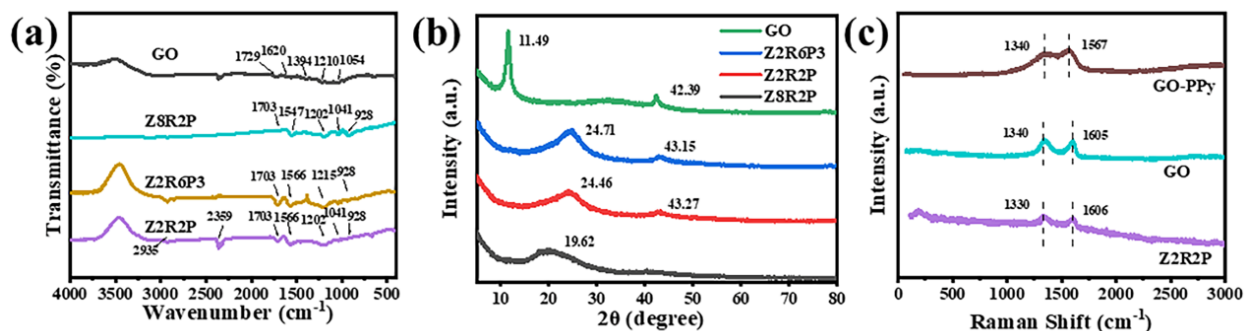


Fig. 2. FT-IR, XRD and Raman spectrums of GO, Z2R2P, Z8R2P and Z2R6P3.

FT-IR is used to confirm and track the formation of chemical bonds during the modification process. Fig. 2(a) shows the FT-IR spectra of GO, Z2R2P, Z8R2P and Z2R6P3. The peaks at 1620 and 1729 cm⁻¹ in the spectrum of GO were assigned to the stretching vibration of C=O bond and the stretching vibration of C=C bond, respectively. Other peaks at 1394, 1210 and 1054 cm⁻¹ were assigned to the deformation vibration of C-O-H bond and the stretching vibration of C-H and C-O bonds.

Therefore, these results indicate that graphite surface is endowed with oxygen functional groups in the process of oxide to GO. After the hydrothermal reaction between GO and $\text{Zn}(\text{NO}_3)_2$, the containing oxygen functional groups on the surface of GO gradually disappeared, New absorption peak appeared, for example, C=C (1729 cm^{-1}), C-O-H (1394 cm^{-1}) and C-O (1054 cm^{-1}), etc. The peaks at 1547 , 1202 and 1041 cm^{-1} in the spectrum of Z8R2P were assigned to the vibration of pyrrole ring and the tensile vibration of antisymmetric C-N and C-H bonds [65, 66], respectively. In addition, the peaks at 900 , and 928 cm^{-1} were related to the doped PPy [67] and ZnO [68], respectively. Altering the mass ratio of ZnO, GO and PPy, the peak locations in the spectra of Z2R2P and Z8R2P changed slightly compared to that of Z2R6P3, indicating that Z2R2P, Z8R2P and Z2R6P3 were successfully synthesized.

Fig. 2(b) shows the XRD patterns of GO, Z2R2P, Z8R2P and Z2R6P3. The characteristic peak of GO appeared at $2\theta = 11.6^\circ$, corresponding to the crystal plane (001). Owing to the doping of ZnO and PPy, the original characteristic peak that belonged to GO disappeared, and the new characteristic peaks appeared at $2\theta = 20^\circ$, 23° and 24° for Z2R2P, Z8R2P and Z2R6P3, respectively. The above results were consistent with the characteristic peak of ZnO_RGO_PPy [69], revealing that GO had formed this disordered accumulation in the synthesis of ternary composites. Raman spectra were used to analyze the structure of composites, especially for carbon materials. The Raman spectra of GO, GO-PPy and ZnO_RGO_PPy are shown in Fig. 2(c). According to the calculation of energy band, the values of I_D/I_G belonged to GO, PPy, and Z8R2P were 1.84, 1.39 and 2.57, respectively. Therefore, this indicated that the disorder degree of GO was improved greatly owing to the doping of ZnO and PPy.

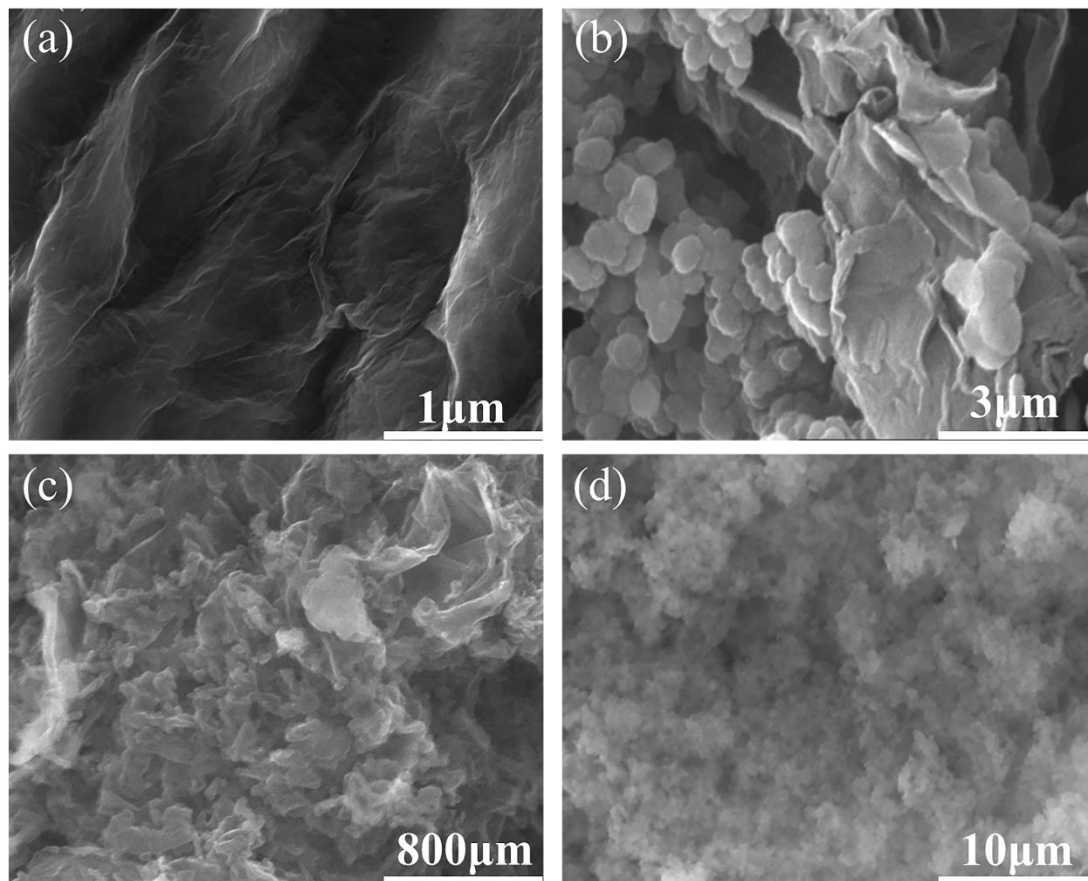


Fig. 3. The FESEM morphologies of GO、Z2R2P、Z8R2P and Z2R6P3.

FESEM is used to characterize the morphology and microstructure of the prepared composites. Fig. 3 shows the FESEM morphologies of GO, Z2R2P, Z8R2P and Z2R6P3. According to Fig. 3(a), GO displays a typical wrinkle structure. It was worth noting that the three proportions of ZnO_RGO_PPy had still wrinkle structure, which indicated that the lamellar structure of GO was not damaged during the modification process. The relatively rougher surfaces of these three composites (Z2R2P, Z8R2P and Z2R6P3) as depicted in Fig. 3(b-d) indicated that PPy had polymerized and formed a thin film on the nanosheets. Moreover, the granular ZnO on the surface of Z8R2P appeared more obviously compared to the other two ZnO_RGO_PPy, which was attributed to the high content of ZnO for Z8R2P composites.

3.2. Mechanical properties of the composite coatings

The impact resistance properties of WEP, Z2R2P/WEP, Z8R2P and Z2R6P3/WEP coatings were tested according to GB/T 1732-2020. The impact height of the drop hammer in this experiment was set at 50 cm. No obvious cracks, spalling and other defects were found in all coatings according to the observation with the aid of a magnifying glass. This indicated that all composite coatings had excellent impact resistance property and met the requirements of the practical application. The adhesion property of WEP, Z2R2P/WEP, Z8R2P and Z2R6P3/WEP coatings was tested according to GB/T 1720-2020. The adhesion of all composite coatings showed as grade 1, indicating excellent interfacial adhesion property between coating and substrate.

The flexibility of WEP, Z2R2P/WEP, Z8R2P and Z2R6P3/WEP coatings was tested according to GB/T 1731-2020. These composite coatings were checked carefully with a quadruple magnifying glass after the test was complete. No damages such as reticulation, crack and peeling were found according to the observation result, indicating excellent flexibility property of the composite coatings.

3.3. *Corrosion resistance property of the composite coatings*

EIS measurements are used to evaluate the corrosion protection property of the composite coatings during immersion in 3.5 wt% NaCl solution. Fig. 4 shows the Nyquist plots of the WEP, Z2R2P/WEP, Z8R2P/WEP and Z2R6P3/WEP coatings after being immersed in 3.5 wt% NaCl for 24 h, 120 h, 240 h and 94 d. In the Nyquist plots, all plots presented the similar shape, which were semicircle but with different diameters. The flattened capacitive semicircle was an indicative of frequency dispersion owing to the defects in the WEP coatings [69-71]. The capacitive semicircle of

the Nyquist plots had been gradually decreased for all the prepared coatings by prolonging the immersion time, indicating that the corrosion resistance of the coatings has been gradually deteriorated. At the early period of immersion (24 h), the sequence of the capacitive characteristic diameter for the composite coating was $Z_{8R2P}/WEP > Z_{2R2P}/WEP > WEP > Z_{2R6P3}/WEP$, indicating that the Z_{8R2P}/WEP coating had the best corrosion protection. When the immersion time was up to 120 h, the sequence of the capacitive characteristic diameters for the composite coatings had not changed compared to that at 24 h immersion time. With prolonging the immersion time to 240 h, the above sequence had no change, and Z_{8R2P}/WEP still exhibited the largest capacitive characteristic compared to other coatings. After 94 days of immersion, the diameter of flattened capacitive semicircle in Z_{8R2P}/WEP coating still exhibited the largest while that of other coatings had an obvious decrease. This indicated that Z_{8R2P}/WEP coating had the best corrosion protection performance through the whole immersion period of 94 d.

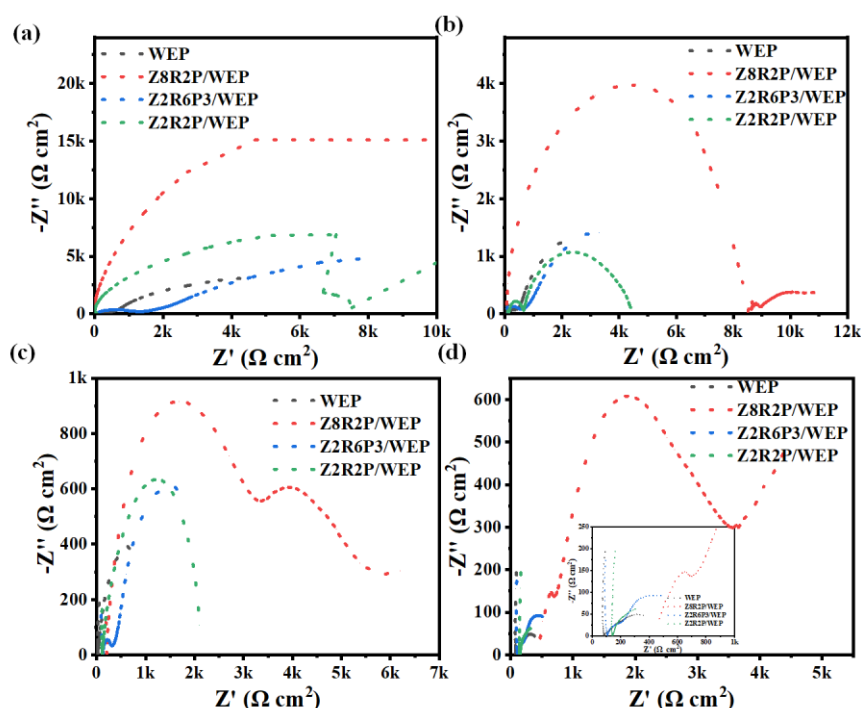


Fig. 4. The Nyquist plots of the WEP, Z8R2P/WEP, Z2R6P3/WEP and Z2R2P/WEP coatings after immersed in 3.5 wt% NaCl for (a) 24 h, (b) 120 h, (c) 240 h and (d) 94 d.

Fig.5 shows the Bode modulus plots of the WEP、Z2R2P/WEP、Z8R2P/WEP and Z2R6P3/WEP coatings after immersed in 3.5 wt% NaCl for 24 h, 120 h, 240 h and 94 d. The impedance at the lowest frequency ($Z_{0.01\text{Hz}}$) reflects the barrier ability of the coatings [72-74]. At the early stage of immersion (24 h), the $Z_{0.01\text{Hz}}$ values of WEP and Z2R6P3/WEP coatings were 9.91×10^3 and $9.20 \times 10^3 \Omega \text{ cm}^2$, respectively. Surprisingly, the $Z_{0.01\text{Hz}}$ values of Z8R2P/WEP and Z2R2P/WEP coatings were up to 1.17×10^5 and $9.21 \times 10^4 \Omega \text{ cm}^2$, which was increased by two orders of magnitude. This revealed that the coating could impede the current flow from anodic to cathodic. However, the $Z_{0.01\text{Hz}}$ values of WEP, Z2R6P3/WEP and Z2R2P/WEP coatings sharply dropped to less than $5 \times 10^3 \Omega \text{ cm}^2$ after 120 h of immersion. This indicated the rapid deterioration of barrier for these composite coatings and WEP coating since the aggressive species penetrated through the coating matrix to the mild steel surface. As expected, the $Z_{0.01\text{Hz}}$ value of Z8R2P/WEP coating was maintained at $10^4 \Omega \text{ cm}^2$ after 120 h of immersion, which was significantly higher compared to other coatings. Moreover, with prolonging the immersion time to 94 d, the $|Z|_{0.01\text{Hz}}$ value of Z8R2P/WEP coating was $4.45 \times 10^3 \Omega \cdot \text{cm}^2$, which had no obvious decrease than that after 240 h of immersion. While the $|Z|_{0.01\text{Hz}}$ values of other coatings were less than $0.5 \times 10^3 \Omega \cdot \text{cm}^2$, which were far lower than that of Z8R2P/WEP coating. This indicated that Z8R2P/WEP coating formed tortuous diffusion pathways for aggressive species. Regardless of the immersion times, Z8R2P/WEP coating showed the largest $Z_{0.01\text{Hz}}$ values while the neat WEP coating had the lowest $Z_{0.01\text{Hz}}$ values, there was a difference of more than 6 times of magnitude between them. This indicates that Z8R2P/WEP had the best anticorrosion property and the neat WEP coating

had the worst anticorrosion property. This phenomenon was in an agreement with the Nyquist diagrams during the whole immersion periods.

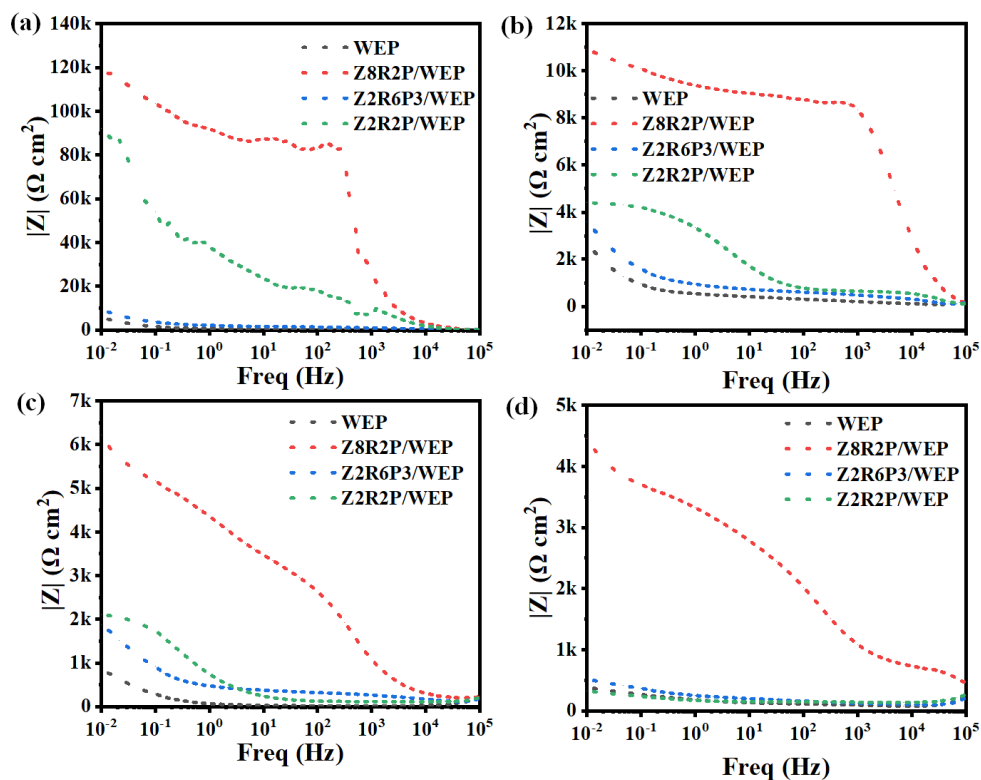


Fig. 5. The Bode modulus plots of the WEP、Z2R2P/WEP、Z8R2P/WEP and Z2R6P3/WEP coatings after immersed in 3.5 wt% NaCl for (a) 24 h, (b) 120 h, (c) 240 h and (d) 94 d.

In the Bode phase plots (Fig. 6), the low frequency constant reveals the corrosion response of the mild steel, the high frequency constant reveals the capacitance and defects of the coatings. Thus, a coating with two-time constants in Bode phase spectrum indicates that the aggressive species has contacted the surface of the mild steel during immersion periods. At the beginning of immersion (24 h), the time constant of the neat WEP appeared at the low frequency while the time constant of composite coating appeared at the high frequency. Due to the corrosion response at the low frequency, the corrosion reaction of WEP coating had begun at the initial stage. While Z2R2P/WEP and

Z8R2P/WEP coatings appeared at high frequency region, its phase angle was close to 90 °. This indicated that the Z2R2P/WEP and Z8R2P/WEP coatings prevented the corrosive media from diffusing through the coating and entering the mild steel surface.

In addition, compared with neat WEP and the Z2R6P3/WEP coatings, Z2R2P/WEP and Z8R2P/WEP coatings had the higher $\phi_{105\text{Hz}}$ value, indicating that these composite coatings had a better barrier ability. The time constant of Z2R2P/WEP coating moved to the low frequency direction, which indicated that the corrosion occurred after 120 h of immersion. With the immersion prolonged to 240 h, the time constant of Z2R2P /WEP coating further moved to the low frequency direction while the time constant of Z8R2P/WEP coating still appeared at the high frequency and the capacitive response of the coatings existed. While WEP coating showed the second time constant, indicating that the corrosive mediums had passed through the coating and entered the interface between metal and coating at this stage. Moreover, after 94 d of immersion, higher phase angle at high frequency range for Z8R2P/WEP coating was obtained compared to other coatings. These results indicated that Z8R2P/WEP coating had the best corrosion resistance property after the long-time immersion. The abnormal phenomenon in the Bode diagram is a corrosion system with multiple time constants. The time constant in the high frequency region corresponds to the capacitive response of the coating, and the time constant in the middle and low frequency region corresponds to the corrosion response of the substrate. As shown in Fig. 6 in the manuscript, the time constants for different immersion time of Z8R2P/WEP coating appear in the high frequency region, and the capacitive response of the coating shows that the coating has good barrier properties.

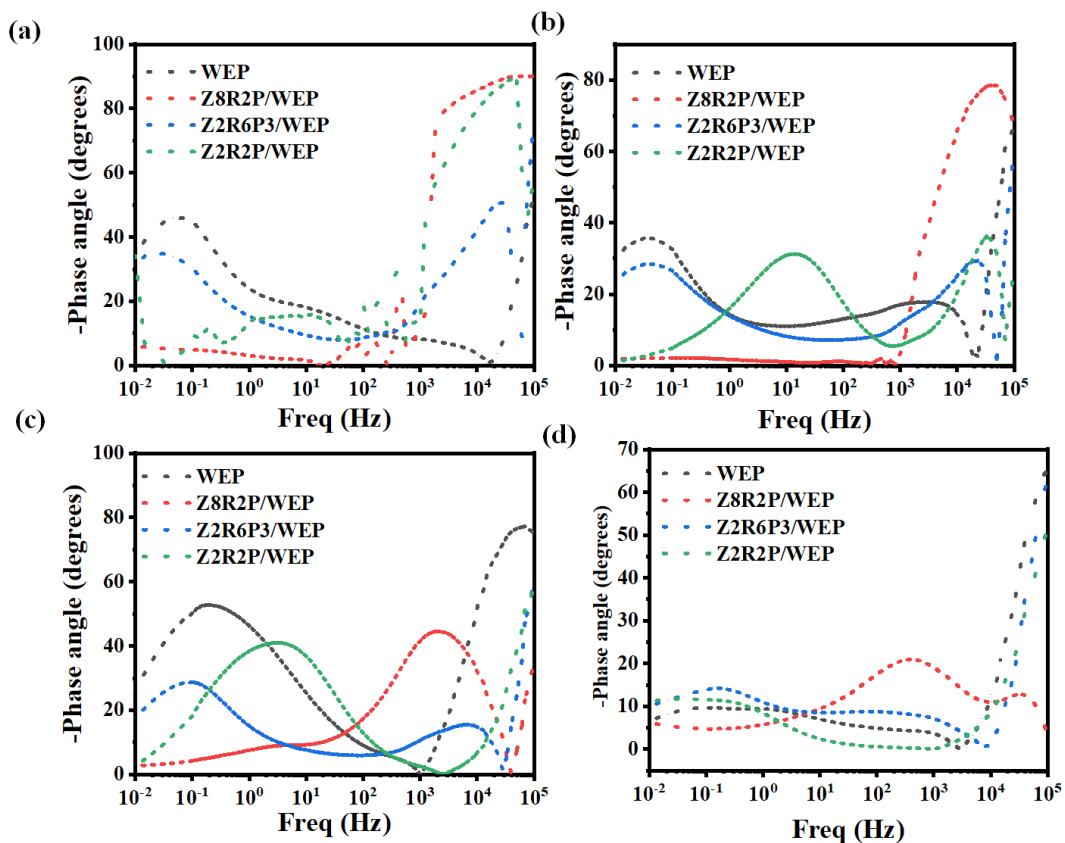


Fig. 6. The Bode phases plots of the WEP、Z2R2P/WEP、Z8R2P/WEP and Z2R6P3/WEP coatings after immersed in 3.5 wt% NaCl for (a)24 h, (b)120 h, (c)240 h and (d) 94 d.

Tafel plots and corresponding polarization parameters of WEP, Z2R2P/WEP, Z2R6P3/WEP and Z8R2P/WEP coatings are shown in Fig. 7 and Table S1. Generally, the lower i_{corr} the material, the lower trend of corrosion and oxidation. At the early stage of immersion, the i_{corr} values of WEP and Z2R6P3/WEP were 9.426×10^{-8} and 4.817×10^{-8} A/cm² while that of Z8R2P/WEP was up to 7.750×10^{-9} A/cm², which was one order of magnitude lower than WEP coating. With the immersion being prolonged to 120 h, the i_{corr} values of WEP、Z2R2P/WEP and Z2R6P3/WEP coatings were increased by an order of magnitude after 120 h of immersion. While Z8R2P/WEP coating had no obvious change at this immersion stage, with the time being prolonged to 240 h, the i_{corr} value of Z8R2P/WEP coating was 1.583×10^{-7} A/cm², which was not significantly improved compared with the initial immersion

period. This indicated that Z8R2P could effectively impede the current flow from anodic to cathodic, thus showed the best corrosion protection property. In addition, the corrosion rate (d) of WEP, Z2R2P/WEP and Z2R6P3/WEP coatings were 1.12×10^{-3} , 1.99×10^{-4} and 5.43×10^{-3} mm/year, respectively. However, the corrosion rate of Z8R2P/WEP coating was 9.12×10^{-5} mm/year, which was two order of magnitude lower compared with WEP and Z2R6P3/WEP coatings, and one order of magnitude lower than Z2R2P/WEP coating, respectively. Moreover, after 94 d of immersion, Z8R2P/WEP coating exhibited smaller current density and greater potential compared to other coatings as shown in Fig. 7(d). This indicated that Z8R2P/WEP coating had the long-term anticorrosion property, which was attributed to the fact that more Zn^{2+} could lead to a more dense passive film on the surface of the substrate.

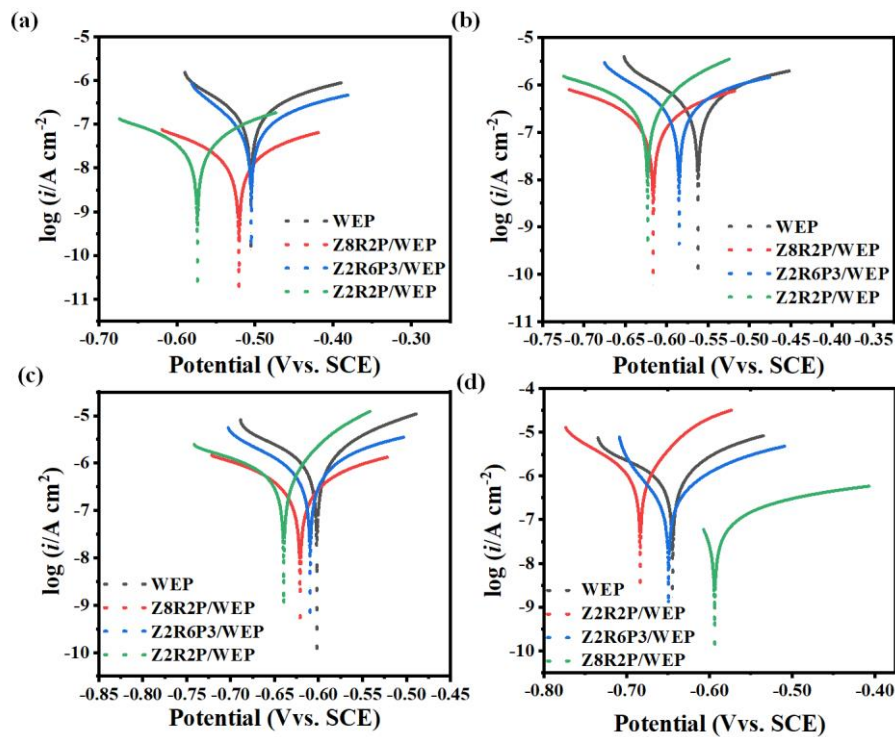


Fig. 7. The Tafel plots of the WEP, Z2R2P/WEP, Z8R2P/WEP and Z2R6P3/WEP coatings after immersed in 3.5 wt% NaCl for (a) 24 h, (b) 120 h, (c) 240 h and (d) 94 d.

ZSimpWin was used to simulate equivalent circuit based on the EIS data of all coatings during the immersion period. In the fitting process, the appropriate equivalent model was selected based on the small Chi-Square value, which was consistent with the immersion period. The fitted equivalent circuit models and corresponding electrochemical parameters are shown in Fig. S1 and Table S2. The corresponding electrochemical parameter mainly include R_s , R_c , R_{ct} , C_c and C_{dl} , which represent the solution resistance between calomel reference electrode and working electrode, composite coating resistance, charge transfer resistance between metal surface and NaCl solution, composite coating capacitance and the double electric layer. Combined with the data analysis of electrochemical impedance, the model as shown in Fig. S1(a) is suitable for all coating during 120 h of immersion, and the model as shown in Fig. S2(b) is suitable for all coatings after 240 h of immersion. All the Chi-Square values for the fitting results were little, which showed that the fitting results of the equivalent circuit were reliable.

At the early stage of immersion (24 h), the R_{ct} values of WEP and Z2R6P3/WEP coatings were 3.93×10^3 and $6.02 \times 10^3 \Omega \cdot \text{cm}^2$ while that of Z8R2P/WEP coating was $9.02 \times 10^3 \Omega \cdot \text{cm}^2$, which was increased by 23 times of magnitudes than WEP coating, and 11.6 times of magnitudes than Z2R6P3/WEP coating. This depicted that Z8R2P/WEP coating had the best physical barrier capability after 24 h of immersion. After 240 h of immersion, the R_{ct} values of WEP, Z2R2P/WEP, Z2R6P3/WEP and Z8R2P/WEP coatings had a significant decrease while that of Z8R2P/WEP coating still was $9.10 \times 10^3 \Omega \cdot \text{cm}^2$, which was improved by 5.4 times of magnitudes than WEP coating. With increasing the immersion time to 240 h, the aggressive corrosive media have entered the interface between the metal substrate and the coating. Then the equivalent circuit model as shown in Fig. S1(b) was suitable for all the composite coatings at this immersion stage. The R_s , R_c , and R_{ct} values of Z8R2P/WEP coating were

0.25×10^3 , 2.49×10^3 and $2.16 \times 10^3 \Omega \cdot \text{cm}^2$, which were much higher than that of other coatings. Regardless of immersion time, Z8R2P/WEP coating had the largest R_{ct} value compared to WEP, Z2R2P/WEP and Z2R6P3/WEP coatings, which indicated that it had the best corrosion protection property.

3.4. Salt spray test of the composite coatings

Fig. 8 shows the digital photos of WEP, Z2R2P/WEP, Z2R6P3/WEP and Z8R2P/WEP coatings after salt spray test for 1, 10, 30 and 50 days. After one day of salt spray test, slight rust appeared at the cross scratches on the surface of all the specimens. After 10 days of salt spray test, rust appeared in most areas of WEP and Z2R6P3/WEP. Then some rust occurred around the scratches center of Z2R2P/WEP coating. However, for Z8R2P/WEP coating, slight rust still appeared around the scratches. After 30 days of salt spray test, WEP, Z2R2P/WEP and Z2R6P3/WEP coatings were peeled off, and deep rust appeared, especially for WEP coating. Meanwhile, Z8R2P/WEP coating had the wider and deeper rust compared to that after 10 days of test but retained the relatively complete coating. After 50 days of salt spray test, many cracks appeared in the WEP coating, and the metal substrate even leaked in some areas, which indicated that WEP coating had lost the corrosion protection ability. Z2R2P/WEP coating was peeled off around the center of scratches, while the coating below was still relatively complete. The whole surface of Z2R6P3/WEP coating was covered by massive rusts and the areas of peel off were increased. While Z8R2P/WEP coating showed relatively complete, some slight rusts appeared in local areas except for the rust around the scratches. Regardless of salt spray test time, Z8R2P/WEP coating had the best integrity of coating compared with other coatings, indicating that Z8R2P/WEP coating had the best corrosion protection performance.

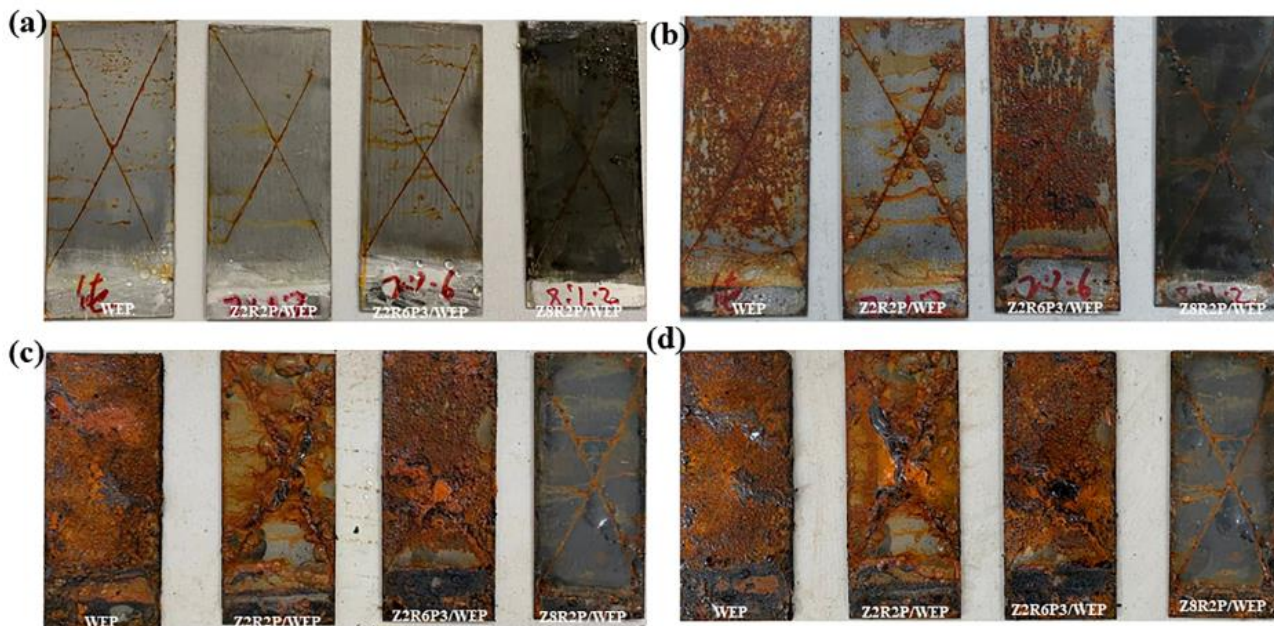


Fig. 8. Digital photos of WEP, Z2R2P/WEP, Z2R6P3/WEP and Z8R2P/WEP coatings after salt spray test for (a)1, (b)10, (c)30 and (d)50 days.

3.5. Corrosion products

To reveal the corrosion protective mechanism of ZnO-RGO-PPy/WEP composite coating, the corrosion products were characterized. In this study, the corrosive products on the mild steel beneath these composites were characterized by FESEM and XRD. The XRD patterns of WEP and Z8R2P/WEP coatings after 10-day immersion in 3.5 wt% NaCl solution are shown in Fig. S2. The patterns of WEP coating appeared at $2\theta = 45^\circ$, 65° and 82.5° , which mainly came from the Fe element contained in the metal substrate. However, the patterns of Z8R2P/WEP coating appeared at $2\theta = 30^\circ$ and 65° , revealing that the rust layers were composed of Fe_2O_3 and FeOOH . This indicated that Z8R2P could promote the passive coating on the surface of metal substrate. Fig. S3 shows the FESEM morphologies for WEP and Z8R2P/WEP coatings. WEP coating as shown in Fig. S3(a) shows an obvious delamination. The traces left by grinding and polishing were still clearly observed, then

corrosive media entered the metal surface along these traces. For Z8R2P/WEP coating as shown in Fig. S3(b), the surface appeared excellent distributed nanosheets, which formed a dense barrier layer and thus could effectively prevent corrosive media from entering the metal surface, thus improved the barrier ability of the coating.

3.6. Corrosion protection mechanism

The schematic diagram of corrosion protection mechanism of ZnO-RGO-PPy/WEP composite coating is shown in Fig. 9. During the long-time immersion in 3.5 wt% NaCl solution, corrosive media gradually penetrated into the interior of the coating and reached the interface between the metal substrate and coating, then a series of redox reactions were induced on the metal surface. This destroyed the structure and properties of metal substrate, leading to a gradual loss of its basic properties. As a physical barrier layer, WEP coating protected the metal substrate from corrosive media entering interface between the metal surface and coating. However, with the extension of immersion time, corrosive media gradually permeated through the coating and diffused into the surface of metal substrate, thus inducing the corrosion reaction. The nanosheets contained in Z8R2P were evenly dispersed into the coating system, improved the physical barrier ability of the composite coating owing to the more tortuous path of corrosive media. In addition, ZnO contained in Z8R2P dissociated more Zn^{2+} ions, and formed a dense passive film on the metal surface, which effectively prevented the further diffusion of media into the metal surface. This might be the reason why Z8R2P/WEP coating showed the best corrosion resistance property. Moreover, PPy contained in Z8R2P accepted the released electrons from the dissolution of the metal, which was conducive to the formation of passive film

composed of Fe_2O_3 on the metal surface. Therefore, excellent corrosion resistance of Z8R2P/WEP coating was mainly due to the synergistic effect of RGO, ZnO and PPy.

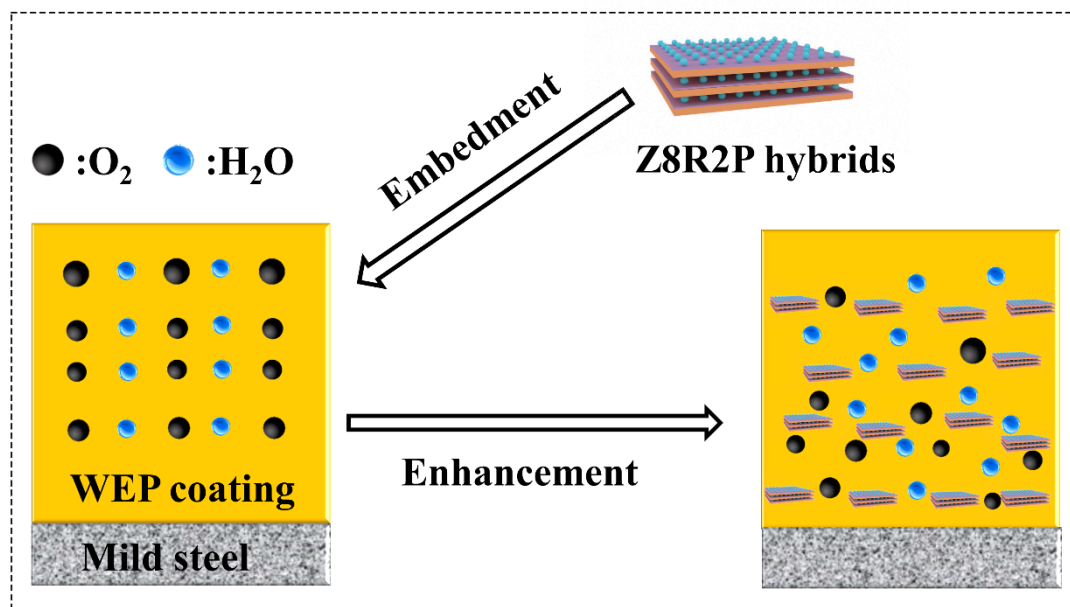


Fig. 9. Schematic representation of protective mechanism of ZnO-RGO-PPy/WEP composite coating.

4. Conclusion

In conclusion, the nanohybrids of Z2R2P, Z2R6P3 and Z8R2P were prepared successfully through hydrothermal treatment, as confirmed by the FT-IR, XRD, Raman and FESEM. The corrosion resistance performance of WEP coatings without and with Z2R2P, Z2R6P3 and Z8R2P on mild steels was confirmed by Tafel curves, EIS and salt spray measures. In regards of less immersion period, the composite coating with Z8R2P exhibited the highest value of $|Z|_{0.01\text{Hz}}$, the lowest corrosion current density and the largest value of R_{ct} . Even for 94 days of immersion period, the $|Z|_{0.01\text{Hz}}$ value of Z8R2P/WEP coating was $4.45 \times 10^3 \Omega \cdot \text{cm}^2$. It proved that Z8R2P/WEP possessed the long superior

anticorrosive ability. The mechanism of synergistic protection was attributed to the barrier effects of RGO, chemical passivation of ZnO and acceptance of the released electrons by PPy. Our study reveals that this environment friendly ZnO-RGO-PPy can be applied not only in the field of corrosion resistance but also in other industry areas, such as supercapacitor [75-77], conductor [78-81], sensors [82-84], and electromagnetic interference (EMI) shielding [85-87].

Acknowledgement

This research is supported by the science foundation of national key laboratory of science and technology on advanced composites in special environments. The authors would like to thank the Deanship of Scientific Research at Umm Al-Qura University for supporting this work by Grant Code: (22UQU4320141DSR14).

Declarations

Conflict of interest the authors declare no competing interests.

References

- [1] T.Z. Xin, Y.H. Zhao, R. Mahjoub, J.X. Jiang, A. Yadav, K. Nomoto, R.M. Niu, S. Tang, F. Ji, Z. Quadir, D. Miskovic, J. Daniels, W.Q. Xu, X.Z. Liao, L.Q. Chen, K. Hagihara, X.Y. Li, S. Ringer, M. Ferry, Ultrahigh specific strength in a magnesium alloy strengthened by spinodal decomposition, *Science Advances*, 7 (2021) eabf3039.
- [2] L.-Q. Chen, Y. Zhao, From classical thermodynamics to phase-field method, *Progress in Materials Science*, in press (2021) 10.1016/j.pmatsci.2021.100868.
- [3] M. Song, J. Wang, L. Yuan, C. Luan, Z. Zhou, Investigation on Crack Recovery Behavior of Engineered Cementitious Composite (ECC) Incorporated Memory Alloy Fiber at Low Temperature, *ES Materials & Manufacturing*, 17 (2022) 23-33.
- [4] S.Z. Gao, Xiaohui; Fu, Qi; et al., Highly transmitted silver nanowires-SWCNTs conductive flexible film by nested density structure and aluminum-doped zinc oxide capping layer for flexible amorphous silicon solar cells, *Journal of Materials Science & Technology*, 126 (2022) 152-160.
- [5] Y. Zhao, K. Liu, H. Hou, L.-Q. Chen, Role of interfacial energy anisotropy in dendrite orientation in Al-Zn alloys: A phase field study, *Materials & Design*, 216 (2022) 110555.
- [6] S. S, e.N. S, B. Murthy, S. Sharma, A.A. Prasanna, A.C. J., Microstructure and Mechanical Properties of Annealed Quinary Ni-Mn-Sn-Fe-In Heusler Alloy, *Engineered Science*, 17 (2022) 303-308.
- [7] S. Mishra, P. Chaudhary, B.C. Yadav, A. Umar, P. Lohia, D.K. Dwivedi, Fabrication and Characterization of an Ultrasensitive Humidity Sensor Based on Chalcogenide Glassy Alloy Thin Films, *Engineered Science*, 15 (2021) 138-

- [8] J. Yan, H. Wei, H. Xie, X. Gu, H. Bao, Seeking for Low Thermal Conductivity Atomic Configurations in SiGe Alloys with Bayesian Optimization, *ES Energy & Environment*, 8 (2020) 56-64.
- [9] L. Shanmugam, M.E. Kazemi, J. Yang, Improved Bonding Strength Between Thermoplastic Resin and Ti Alloy with Surface Treatments by Multi-step Anodization and Single-step Micro-arc Oxidation Method: A Comparative Study, *ES Materials & Manufacturing*, 3 (2019) 57-65.
- [10] L. Lin, X. Xian, Z. Zhong, K. Song, C. Wang, G. Wang, Y. Wu, P.K. Liaw, Microstructure and compression properties of a dual-phase FeCoCrMn high-entropy alloy, *Advanced Composites and Hybrid Materials*, 5 (2022) 1508-1515.
- [11] P.R. Jadhav, B.R. Sridhar, M. Nagaral, J.I. Harti, Mechanical behavior and fractography of graphite and boron carbide particulates reinforced A356 alloy hybrid metal matrix composites, *Advanced Composites and Hybrid Materials*, 3 (2020) 114-119.
- [12] W. Chen, Y. Zhao, S. Yang, D. Zhang, H. Hou, Three-dimensional phase-field simulations of the influence of diffusion interface width on dendritic growth of Fe-0.5 wt.%C alloy, *Advanced Composites and Hybrid Materials*, 4 (2021) 371-378.
- [13] G. Qiao, S. Wang, X. Wang, X. Chen, X. Wang, H. Cui, Ni/Co/black phosphorus nanocomposites for Q235 carbon steel corrosion-resistant coating, *Advanced Composites and Hybrid Materials*, 5 (2022) 438-449.
- [14] M. Farahmandian, M. Saidi, S. Fazlinejad, Synthesis and characterization of nickel-cobalt spin coatings reinforced with carbon nanotubes: microstructural properties, microhardness, and corrosion resistance, *Advanced Composites and Hybrid Materials*, 5 (2022) 1490-1507.
- [15] H. Song, Q. Zhang, Y. Zhang, Y. Wang, Z. Zhou, P. Zhang, B. Yuan, Waterborne polyurethane/3-amino-polyhedral oligomeric silsesquioxane (NH₂-POSS) nanocomposites with enhanced properties, *Advanced Composites and Hybrid Materials*, 4 (2021) 629-638.
- [16] H. Du, X. Ren, D. Pan, Y. An, Y. Wei, X. Liu, L. Hou, B. Liu, M. Liu, Z. Guo, Effect of phosphating solution pH value on the formation of phosphate conversion coatings for corrosion behaviors on AZ91D, *Advanced Composites and Hybrid Materials*, 4 (2021) 401-414.
- [17] J. Zhang, Z. Kang, D. Hou, B. Dong, H. Ma, Wavelet Power and Shannon Entropy Applied to Acoustic Emission Signals for Corrosion Detection and Evaluation of Reinforced Concrete, *ES Materials & Manufacturing*, 16 (2022) 46-55.
- [18] A.M. Madhusudhana, K.N.S. Mohana, M.B. Hegde, S.R. Nayak, K. Rajitha, N.K. Swamy, Functionalized graphene oxide-epoxy phenolic novolac nanocomposite: an efficient anticorrosion coating on mild steel in saline medium, *Advanced Composites and Hybrid Materials*, 3 (2020) 141-155.
- [19] J. Liu, J. Zhang, J. Tang, L. Pu, Y. Xue, M. Lu, L. Xu, Z. Guo, Polydimethylsiloxane Resin Nanocomposite Coating with Alternating Multilayer Structure for Corrosion Protection Performance, *ES Materials & Manufacturing*, 10 (2020) 29-38.
- [20] R.T.T. Jalgham, Theoretical, Monte Carlo Simulations and QSAR Studies on Some Triazole Derivatives as Corrosion Inhibitors for Mild Steel in 1 M HCl, *ES Energy & Environment*, 13 (2021) 37-49.
- [21] R.B. Ashok, C.V. Srinivasa, B. Basavaraju, Study on morphology and mechanical behavior of areca leaf sheath reinforced epoxy composites, *Advanced Composites and Hybrid Materials*, 3 (2020) 365-374.
- [22] U.S. Gupta, M. Dhamarika, A. Dharkar, S. Tiwari, R. Namdeo, Study on the effects of fibre volume percentage on banana-reinforced epoxy composite by finite element method, *Advanced Composites and Hybrid Materials*, 3 (2020) 530-540.
- [23] Z. Chen, Y. Huang, Preparation and performance of fumed silica-stabilized epoxy resin pickering emulsion for basalt fiber-sizing agents, *Advanced Composites and Hybrid Materials*, 4 (2021) 1205-1214.

- [24] S.Y. Nayak, S.S. B, C. Ch, r.R. Kini, M.T.H. Sultan, F.S. Shahar, Experimental Investigation into Mechanical Properties of Coconut Shell Powder Modified Epoxy/3D E-Glass Composites, *Engineered Science*, 20 (December 2022) In Progress (2022).
- [25] H. Duan, C. Zhuang, F. Mei, C. Zeng, R.A. Pashameah, M. Huang, E. Alzahrani, J. Gao, Y. Han, Q. Yu, Z. Wang, Benzyl(4-fluorophenyl)phenylphosphine oxide-modified epoxy resin with improved flame retardancy and dielectric properties, *Advanced Composites and Hybrid Materials*, 5 (2022) 776-787.
- [26] Q. Zhu, E. Li, X. Liu, W. Song, M. Zhao, L. Zi, X. Wang, C. Liu, Synergistic effect of polypyrrole functionalized graphene oxide and zinc phosphate for enhanced anticorrosion performance of epoxy coatings, *Composites Part A: Applied Science and Manufacturing*, 130 (2020) 105752.
- [27] J. Han, T. Liu, S. Zhang, C. Hao, J. Xin, B. Guo, J. Zhang, Hyperbranched Polymer Assisted Curing and Repairing of an Epoxy Coating, *Industrial & Engineering Chemistry Research*, 58 (2019) 6466-6475.
- [28] X. Jia, B. Shen, Z. Chen, L. Zhang, W. Zheng, High-Performance Carbonized Waste Corrugated Boards Reinforced with Epoxy Coating as Lightweight Structured Electromagnetic Shields, *ACS Sustainable Chemistry & Engineering*, 7 (2019) 18718-18725.
- [29] Y. Peng, A.E. Hughes, J.I. Mardel, G.B. Deacon, P.C. Junk, M. Forsyth, B.R.W. Hinton, A.E. Somers, Leaching Behavior and Corrosion Inhibition of a Rare Earth Carboxylate Incorporated Epoxy Coating System, *ACS Applied Materials & Interfaces*, 11 (2019) 36154-36168.
- [30] M. Sabu, E. Bementa, Y. Jaya Vinse Ruban, S. Ginil Mon, A novel analysis of the dielectric properties of hybrid epoxy composites, *Advanced Composites and Hybrid Materials*, 3 (2020) 325-335.
- [31] H. Xia, J. Li, K. Wang, X. Hou, T. Yang, J. Hu, Z. Shi, Superior wear resistance of epoxy composite with highly dispersed graphene spheres, *Advanced Composites and Hybrid Materials*, (2021).
- [32] I. Bustero, I. Gaztelumendi, I. Obieta, M.A. Mendizabal, A. Zurutuza, A. Ortega, B. Alonso, Free-standing graphene films embedded in epoxy resin with enhanced thermal properties, *Advanced Composites and Hybrid Materials*, 3 (2020) 31-40.
- [33] F. Xu, D. Bao, Y. Cui, Y. Gao, D. Lin, X. Wang, J. Peng, H. Geng, H. Wang, Copper nanoparticle-deposited graphite sheets for highly thermally conductive polymer composites with reduced interfacial thermal resistance, *Advanced Composites and Hybrid Materials*, (2021).
- [34] A. An, P. Pai, A.K. Kini, C. Ch, r.R. Kini, S.S. B, Effect of Natural Fibre-epoxy Plies on the Mechanical and Shock Wave Impact Response of Fibre Metal Laminates, *Engineered Science*, 19 (September 2022) In Progress (2022) 292-300.
- [35] M. Cui, S. Ren, H. Zhao, Q. Xue, L. Wang, Polydopamine coated graphene oxide for anticorrosive reinforcement of water-borne epoxy coating, *Chemical Engineering Journal*, 335 (2018) 255-266.
- [36] Q. Zhu, E. Li, X. Liu, W. Song, Y. Li, X. Wang, C. Liu, Epoxy coating with in-situ synthesis of polypyrrole functionalized graphene oxide for enhanced anticorrosive performance, *Progress in Organic Coatings*, 140 (2020) 105488.
- [37] Q. Zhu, Y. Huang, Y. Li, M. Zhou, S. Xu, X. Liu, C. Liu, B. Yuan, Z. Guo, Aluminum dihydric tripolyphosphate/polypyrrole-functionalized graphene oxide waterborne epoxy composite coatings for impermeability and corrosion protection performance of metals, *Advanced Composites and Hybrid Materials*, 4 (2021) 780-792.
- [38] L. Mi, H. Hw, M. Rb, S. Xx, J. X, Z. Xy, Single-step exfoliation, acidification and covalent functionalization of α -zirconium phosphate for enhanced anticorrosion of waterborne epoxy coatings, *Surfaces and Interfaces*, 23 (2021) 100887.
- [39] O.u. Rahman, M. Kashif, S. Ahmad, Nanoferrite dispersed waterborne epoxy-acrylate: Anticorrosive nanocomposite coatings, *Progress in Organic Coatings*, 80 (2015) 77-86.

- [40] B. Jain, A. Hashmi, S. Sanwaria, A.K. Singh, M.A.B.H. Susan, A. Singh, Zinc oxide nanoparticle incorporated on graphene oxide: an efficient and stable photocatalyst for water treatment through the Fenton process, *Advanced Composites and Hybrid Materials*, 3 (2020) 231-242.
- [41] S.H. Khan, B. Pathak, M.H. Fulekar, A study on the influence of metal (Fe, Bi, and Ag) doping on structural, optical, and antimicrobial activity of ZnO nanostructures, *Advanced Composites and Hybrid Materials*, 3 (2020) 551-569.
- [42] N.N. Prabhu, R.B.J. Ch. r. ra, B.V. Rajendra, G. George, A.-H.I. Mourad, B. Shivamurthy, Electrospun ZnO Nanofiber Based Resistive Gas/Vapor Sensors -A Review, *Engineered Science*, 19 (September 2022) In Progress (2022) 59-82.
- [43] B. Ramezanzadeh, M.M. Attar, Studying the effects of micro and nano sized ZnO particles on the corrosion resistance and deterioration behavior of an epoxy-polyamide coating on hot-dip galvanized steel, *Progress in Organic Coatings*, 71 (2011) 314-328.
- [44] B. Ramezanzadeh, E. Ghasemi, M. Mahdavian, E. Changizi, M.H. Mohamadzadeh Moghadam, Covalently-grafted graphene oxide nanosheets to improve barrier and corrosion protection properties of polyurethane coatings, *Carbon*, 93 (2015) 555-573.
- [45] S. Zhang, B. Cheng, Z. Gao, D. Lan, Z. Zhao, F. Wei, Q. Zhu, X. Lu, G. Wu, Two-dimensional nanomaterials for high-efficiency electromagnetic wave absorption: An overview of recent advances and prospects, *Journal of Alloys and Compounds*, 893 (2022) 162343.
- [46] Y. Dong, Q. Liu, Q. Zhou, Time-dependent protection of ground and polished Cu using graphene film, *Corrosion Science*, 90 (2015) 69-75.
- [47] U. Pandey, A.K. Singh, C. Sharma, Development of anti-corrosive novel nickel-graphene oxide-polypyrrole composite coatings on mild steel employing electrodeposition technique, *Synthetic Metals*, 290 (2022) 117135.
- [48] C. Xie, Y. Jia, M. Xue, Z. Yin, Y. Luo, Z. Hong, W. Liu, Anti-corrosion and self-healing behaviors of waterborne polyurethane composite coatings enhanced via chitosan-modified graphene oxide and phosphate intercalated hydrotalcite, *Progress in Organic Coatings*, 168 (2022) 106881.
- [49] N.T. Kirkland, T. Schiller, N. Medhekar, N. Birbilis, Exploring graphene as a corrosion protection barrier, *Corrosion Science*, 56 (2012) 1-4.
- [50] S. Qiu, W. Li, W. Zheng, H. Zhao, L. Wang, Synergistic Effect of Polypyrrole-Intercalated Graphene for Enhanced Corrosion Protection of Aqueous Coating in 3.5% NaCl Solution, *ACS Applied Materials & Interfaces*, 9 (2017) 34294-34304.
- [51] Q. Liu, Y. Lei, Q. Zeng, C. Li, G. Sun, B. You, W. Ren, Hydrogenated castor oil modified graphene oxide as self-thixotropic nanofiller in high solid polyaspartic coatings for enhanced anti-corrosion performance, *Progress in Organic Coatings*, 167 (2022) 106836.
- [52] S. Zhang, B. Cheng, Z. Jia, Z. Zhao, X. Jin, Z. Zhao, G. Wu, The art of framework construction: hollow-structured materials toward high-efficiency electromagnetic wave absorption, *Advanced Composites and Hybrid Materials*, (2022).
- [53] Y. Zhang, L. Chu, Z. Dai, N. Bao, M.B. de Rooij, L. Gao, W. Tan, L. Shen, Synergistically enhancing the performance of cardanol-rich epoxy anticorrosive coatings using cardanol-based reactive diluent and its functionalized graphene oxide, *Progress in Organic Coatings*, 171 (2022) 107060.
- [54] A. Dehghani, A.H. Mostafatabar, G. Bahlakeh, B. Ramezanzadeh, Metal-doped 2D rGO nano-sheets fabrication utilizing plant source bio-molecules and application in the epoxy anti-corrosive coating: Combined experimental and DFT-D modeling investigations, *Progress in Organic Coatings*, 170 (2022) 106938.
- [55] S. Zhou, Y. Wu, W. Zhao, J. Yu, F. Jiang, L. Ma, Comparative corrosion resistance of graphene sheets with different structures in waterborne epoxy coatings, *Colloids and Surfaces A: Physicochemical and Engineering*

Aspects, 556 (2018) 273-283.

[56] L. Gu, S. Liu, H. Zhao, H. Yu, Facile Preparation of Water-Dispersible Graphene Sheets Stabilized by Carboxylated Oligoanilines and Their Anticorrosion Coatings, *ACS Applied Materials & Interfaces*, 7 (2015) 17641-17648.

[57] F. Jiang, W. Zhao, Y. Wu, Y. Wu, G. Liu, J. Dong, K. Zhou, A polyethyleneimine-grafted graphene oxide hybrid nanomaterial: Synthesis and anti-corrosion applications, *Applied Surface Science*, 479 (2019) 963-973.

[58] Y. Zhao, F. Liu, Z. Zhao, P. Bai, Y. Ma, A. Alhadhrami, G.A.M. Mersal, Z. Lin, M.M. Ibrahim, Z.M. El-Bahy, Direct ink printing reduced graphene oxide/KCu7S4 electrodes for high-performance supercapacitors, *Advanced Composites and Hybrid Materials*, 5 (2022) 1516-1526.

[59] S. Pourhashem, M.R. Vaezi, A. Rashidi, Investigating the effect of SiO₂-graphene oxide hybrid as inorganic nanofiller on corrosion protection properties of epoxy coatings, *Surface and Coatings Technology*, 311 (2017) 282-294.

[60] Z. Yu, H. Di, Y. Ma, Y. He, L. Liang, L. Lv, X. Ran, Y. Pan, Z. Luo, Preparation of graphene oxide modified by titanium dioxide to enhance the anti-corrosion performance of epoxy coatings, *Surface and Coatings Technology*, 276 (2015) 471-478.

[61] Z. Yu, H. Di, Y. Ma, L. Lv, Y. Pan, C. Zhang, Y. He, Fabrication of graphene oxide-alumina hybrids to reinforce the anti-corrosion performance of composite epoxy coatings, *Applied Surface Science*, 351 (2015) 986-996.

[62] N.N. Taheri, B. Ramezanzadeh, M. Mahdavian, G. Bahlakeh, In-situ synthesis of Zn doped polyaniline on graphene oxide for inhibition of mild steel corrosion in 3.5wt.% chloride solution, *Journal of Industrial and Engineering Chemistry*, 63 (2018) 322-339.

[63] Y. Ding, J. Zhong, P. Xie, J. Rong, H. Zhu, W. Zheng, J. Wang, F. Gao, L. Shen, H. He, Z. Cheng, Protection of Mild Steel by Waterborne Epoxy Coatings Incorporation of Polypyrrole Nanowires/Graphene Nanocomposites, *Polymers*, 11 (2019).

[64] Q. Zhu, K. Zhang, Y. Huang, R. Liu, Y. Pan, H. Zhang, P. Wang, S. Zhang, D. Pan, Z. Guo, Hydrothermally synthesized ZnO-reduced graphene oxide nanocomposite for enhanced anticorrosion performance of waterborne epoxy coating, *Journal of Nanostructure in Chemistry*, (2022).

[65] Y. Lin, J. Jin, M. Song, Preparation and characterisation of covalent polymer functionalized graphene oxide, *Journal of Materials Chemistry*, 21 (2011) 3455-3461.

[66] M.S. Ahmed, H.S. Han, S. Jeon, One-step chemical reduction of graphene oxide with oligothiophene for improved electrocatalytic oxygen reduction reactions, *Carbon*, 61 (2013) 164-172.

[67] J. Deng, Y. Peng, C. He, X. Long, P. Li, A.S.C. Chan, Magnetic and conducting Fe₃O₄-polypyrrole nanoparticles with core-shell structure, *Polymer International*, 52 (2003) 1182-1187.

[68] B. Yan, Y. Wang, X. Jiang, K. Liu, L. Guo, Flexible Photocatalytic Composite Film of ZnO-Microrods/Polypyrrole, *ACS Applied Materials & Interfaces*, 9 (2017) 29113-29119.

[69] Y. Chen, Z. Zhao, C. Zhang, Structural and electrochemical study of polypyrrole/ZnO nanocomposites coating on nickel sheet synthesized by electrochemical method, *Synthetic Metals*, 163 (2013) 51-56.

[70] Z.Y. Liu, X.G. Li, C.W. Du, Y.F. Cheng, Local additional potential model for effect of strain rate on SCC of pipeline steel in an acidic soil solution, *Corrosion Science*, 51 (2009) 2863-2871.

[71] C. Liu, R.I. Revilla, Z. Liu, D. Zhang, X. Li, H. Terry, Effect of inclusions modified by rare earth elements (Ce, La) on localized marine corrosion in Q460NH weathering steel, *Corrosion Science*, 129 (2017) 82-90.

[72] W. Hao, Z. Liu, W. Wu, X. Li, C. Du, D. Zhang, Electrochemical characterization and stress corrosion cracking of E690 high strength steel in wet-dry cyclic marine environments, *Mater. Sci. Eng.: A*, 710 (2018) 318-328.

[73] Q. Hou, Z. Liu, C. Li, X. Li, The mechanism of stress corrosion cracking of Alloy 690TT in a caustic solution containing lead, *Corrosion Science*, 128 (2017) 154-163.

- [74] H. Qian, D. Xu, C. Du, D. Zhang, X. Li, L. Huang, L. Deng, Y. Tu, J.M.C. Mol, H.A. Terryn, Dual-action smart coatings with a self-healing superhydrophobic surface and anti-corrosion properties, *Journal of Materials Chemistry A*, 5 (2017) 2355-2364.
- [75] G. Li, L. Wang, X. Lei, Z. Peng, T. Wan, S. Maganti, M. Huang, V. Murugadoss, I. Seok, Q. Jiang, D. Cui, A. Alhadhrami, M.M. Ibrahim, H. Wei, Flexible, yet robust polyaniline coated foamed polylactic acid composite electrodes for high-performance supercapacitors, *Advanced Composites and Hybrid Materials*, 5 (2022) 853-863.
- [76] Z. Zhuang, W. Wang, Y. Wei, T. Li, M. Ma, Y. Ma, Preparation of polyaniline nanorods/manganese dioxide nanoflowers core/shell nanostructure and investigation of electrochemical performances, *Advanced Composites and Hybrid Materials*, 4 (2021) 938-945.
- [77] P. Wang, T. Song, H.M. Abo-Dief, J. Song, A.K. Alanazi, B. Fan, M. Huang, Z. Lin, A.A. Altalhi, S. Gao, L. Yang, J. Liu, S. Feng, T. Cao, Effect of carbon nanotubes on the interface evolution and dielectric properties of polylactic acid/ethylene-vinyl acetate copolymer nanocomposites, *Advanced Composites and Hybrid Materials*, 5 (2022) 1100-1110.
- [78] L. Ouyang, W. Huang, M. Huang, B. Qiu, Polyaniline improves granulation and stability of aerobic granular sludge, *Advanced Composites and Hybrid Materials*, 5 (2022) 1126-1136.
- [79] W. Xie, F. Yao, H. Gu, A. Du, Q. Lei, N. Naik, Z. Guo, Magneto-resistive and piezoresistive polyaniline nanoarrays in-situ polymerized surrounding magnetic graphene aerogel, *Advanced Composites and Hybrid Materials*, 5 (2022) 1003-1016.
- [80] H. Li, W. Huang, B. Qiu, H.K. Thabet, D. Alhashmialameer, M. Huang, Z. Guo, Effective removal of proteins and polysaccharides from biotreated wastewater by polyaniline composites, *Advanced Composites and Hybrid Materials*, (2022) in press, <https://doi.org/10.1007/s42114-022-00508-0>.
- [81] J. Guo, Z. Chen, Z.M. El-Bahy, H. Liu, H.M. Abo-Dief, W. Abdul, K.M. Abualnaja, A.K. Alanazi, P. Zhang, M. Huang, G. Hu, J. Zhu, Tunable negative dielectric properties of magnetic CoFe₂O₄/graphite-polypyrrole metacomposites, *Advanced Composites and Hybrid Materials*, 5 (2022) 899-906.
- [82] J. Guo, X. Li, H. Liu, D.P. Young, G. Song, K. Song, J. Zhu, J. Kong, Z. Guo, Tunable magnetoresistance of core-shell structured polyaniline nanocomposites with 0-, 1-, and 2-dimensional nanocarbons, *Advanced Composites and Hybrid Materials*, 4 (2021) 51-64.
- [83] Y. He, M. Zhou, M.H.H. Mahmoud, X. Lu, G. He, L. Zhang, M. Huang, A.Y. Elnaggar, Q. Lei, H. Liu, C. Liu, I.H.E. Azab, Multifunctional wearable strain/pressure sensor based on conductive carbon nanotubes/silk nonwoven fabric with high durability and low detection limit, *Advanced Composites and Hybrid Materials*, (2022) in press, <https://doi.org/10.1007/s42114-022-00525-z>.
- [84] H. Wei, A. Li, D. Kong, Z. Li, D. Cui, T. Li, B. Dong, Z. Guo, Polypyrrole/reduced graphene aerogel film for wearable piezoresistive sensors with high sensing performances, *Advanced Composites and Hybrid Materials*, 4 (2021) 86-95.
- [85] B. Dai, Y. Ma, F. Dong, J. Yu, M. Ma, H.K. Thabet, S.M. El-Bahy, M.M. Ibrahim, M. Huang, I. Seok, G. Roymahapatra, N. Naik, B.B. Xu, J. Ding, T. Li, Overview of MXene and conducting polymer matrix composites for electromagnetic wave absorption, *Advanced Composites and Hybrid Materials*, 5 (2022) 704-754.
- [86] Y. Wang, P. Wang, Z. Du, C. Liu, C. Shen, Y. Wang, Electromagnetic interference shielding enhancement of poly(lactic acid)-based carbonaceous nanocomposites by poly(ethylene oxide)-assisted segregated structure: a comparative study of carbon nanotubes and graphene nanoplatelets, *Advanced Composites and Hybrid Materials*, 5 (2022) 209-219.
- [87] X. Huang, X. Liu, Z. Jia, B. Wang, X. Wu, G. Wu, Synthesis of 3D cerium oxide/porous carbon for enhanced electromagnetic wave absorption performance, *Advanced Composites and Hybrid Materials*, 4 (2021) 1398-1412.